

Microfluidic liquid actuation through ground-directed electric discharge

Carlos Escobedo · David Sinton

Received: 7 April 2011 / Accepted: 3 June 2011 / Published online: 15 June 2011
© Springer-Verlag 2011

Abstract In this article, we present a new technique to actuate liquids in microchannels using ground-directed electric discharge generated by a portable corona device. When an electric discharge is applied, the air in the microchannel is ionized causing a change in the surface energy. The resulting change in the contact angle induces rapid liquid transport through the channel by capillary action. In contrast to established plasma treatment this method employs a ground electrode that guides the electric field. This approach enables rapid treatment of select microchannels and thus provides a means of real-time fluid actuation as opposed to simply a pretreatment process. Instantaneous fluid velocities show power-law dependence with time and fit theoretical models at a contact angle of 65° . Average fluid velocities are on the order of 5 cm/s, and thus channels on the order of 1-cm long are filled in ~ 0.2 s. To demonstrate the potential of this technique for integrated lab-on-a-chip applications, the method was employed in serpentine channel, for on-demand fluid routing, to initiate a mixing process, and through an on-chip integrated microelectrode.

Keywords Electric discharge · Plasma · Microfluidic · Nanofluidic · Contact angle · Capillary flow · Surface tension · Microfluidic liquid actuation · Corona

Electronic supplementary material The online version of this article (doi:10.1007/s10404-011-0831-4) contains supplementary material, which is available to authorized users.

C. Escobedo · D. Sinton (✉)
Department of Mechanical Engineering, University of Victoria,
P.O. Box 3055, STN CSC, Victoria, BC V8W 3P6, Canada
e-mail: dsinton@me.uvic.ca

1 Introduction

A central advantage of microfluidics is the potential to integrate complex analytical functions (Thorsen et al. 2002; Whitesides 2006). Achieving this integration requires real-time fluid control, or actuation, on the scale of individual channels. Existing methods for real-time flow control in an integrated chip include multilayer elastomeric switching valves (Unger et al. 2000), electrokinetic control with integrated electrodes (Horiuchi and Dutta 2006), burst valves for centrifugal microfluidics (Juncker et al. 2002; Kim et al. 2008), and electro-wetting for droplet systems (Fair 2007; Luk and Wheeler 2009). While the simplicity of capillary-valve-based flow control is attractive, it is not possible to dynamically alter the order or timing of fluidic operations.

Surface treatment is commonly required to increase the wetting properties of microfluidic systems to enable filling. One of the most commonly used materials, poly(dimethylsiloxane) (PDMS), is natively hydrophobic and can be rendered hydrophilic by exposure to oxygen plasma (Makamba et al. 2003). Plasma is a particular phase of matter, commonly referred to as ionized gas, wherein gas particles are electrically charged. Plasma can be artificially produced in air around an electrode at sufficiently high potential gradients. Due to the conductive nature of plasma, an electric discharge may occur within the ionized gas cloud (Bittencourt 2004). Exposure to plasma introduces polar groups on the polymer surface resulting in an increase in surface wettability. A natively hydrophobic polymeric surface thus becomes wettable after plasma exposure (Sun et al. 1999; Zenkiewicz 2005). Most commonly, this is achieved prior to chip bonding by exposing the entire chip surface to plasma under vacuum in a plasma oven. An alternative to the oven-based treatment was

presented by Haubert et al. (2006) where a low cost handheld corona discharge device was applied. The device produces a high voltage (10–50 kV) at 4–5 MHz, ionizing the atmospheric pressure air around the electrode which enabled instantaneous oxidation of the proximate chip surface (Zenkiewicz 2005; Thorslund and Nikolajeff 2007).

Active flow control of gases has been achieved using electric discharges in MEMS devices (Hsu et al. 2007). The phenomenon is usually referred to as ionic wind and has been studied since the eighteenth century (Robinson 1962; Kim et al. 2000; Sung Kwon et al. 2003; Chih-Peng et al. 2007). The electric field strength on a sharply shaped electrode exceeding a certain threshold results in the local ionization of the air. The ionized air molecules emerge as a pale purple cloud and have the same electric charge as the electrode. Charge repulsion results in the expansion of the ionized air cloud away from the conductor, creating a net gas flow (Hilpert and Kern 1974). However, this form of flow actuation using an electric discharge is exclusive to gases (Moreau 2007).

For liquid flows in microfluidics, localized treatment of microfluidic structures has been achieved using corona devices (Evju et al. 2004; Zenkiewicz 2005; Thorslund and Nikolajeff 2007). Localized treatment is enabled by the inherent confinement of the electric field around the electrode (Hilpert and Kern 1974; Seimandi et al. 2009). Additionally, electrohydrodynamic flows generated by corona discharge devices have been used for the promotion of microvortices for mixing and particle trapping (Yeo et al. 2006) and for microfluidic blood plasma separation (Arifin et al. 2007). These previous works demonstrate the ability to locally treat microchannel surfaces using electric discharges from a corona device.

In this article, we demonstrate ground-directed electric discharge that enables rapid treatment of select microchannels, providing a means of real-time fluid actuation. The method is characterized through one- and two-dimensional channel flow experiments, and comparison with mathematical models. To demonstrate applicability to integrated lab-on-chip systems, selective liquid routing and the actuation of a mixing process are demonstrated, as is the application of the technique using an integrated microelectrode. In contrast to previous pretreatment methods, this technique enables the direct control, routing, and actuation of microfluidic flows in real time.

2 Theoretical background

Figure 1 shows a schematic representation of microfluidic liquid actuation through ground-directed electric discharge. A basic configuration with a closed all-PDMS microchannel,

a corona electrode and a ground electrode is shown in the schematics of Fig. 1a, b.

Two analytical models outlined below are applied in the analysis of the experimental results. The Hagen–Poiseuille equation for laminar flow can be expressed as:

$$Q = \frac{dV}{dt} = \left(\frac{\pi R^4}{8\eta} \right) \left(\frac{p_0 - p_{\text{int}}}{l} \right) \quad (1)$$

where Q is the flow rate, V is the volume, t is the time, R is the hydrodynamic radius of the microchannel, η is the dynamic viscosity of the liquid, p_0 is the liquid pressure at the entrance of the microchannel, p_{int} is the liquid pressure at the meniscus, and l is the distance from the microchannel

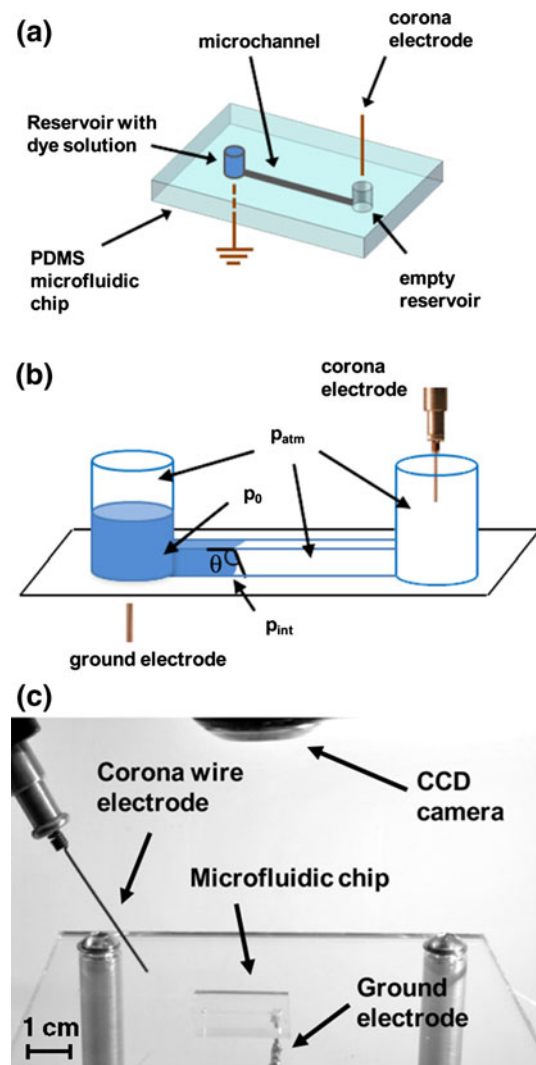


Fig. 1 The ground-directed electric discharge liquid actuation setup. **a** Schematic showing the corona electrode is placed in one of the reservoirs and a ground electrode is placed under the second reservoir containing solution, **b** diagram showing the geometry and parameters relevant to the system, and **c** image of the experimental setup. The acrylic working surface had a 2-mm circular opening for ground electrode access

inlet to the air–liquid interface, or penetration length. The capillary pressure is defined by the Young–Laplace equation as:

$$p_{\text{atm}} - p_{\text{int}} = \frac{2\sigma}{R} \cos\theta \tag{2}$$

where p_{atm} is the atmospheric pressure, σ is the surface tension, and θ is the liquid–gas interface contact angle at the solid. Substituting Eq. 2 in 1 and rearranging the terms the following expression is obtained:

$$\frac{2\sigma}{R} \cos\theta = \left(\frac{8\eta}{R^2}\right) \left(\frac{dl}{dt}\right) + (p_{\text{atm}} - p_{\text{int}}) \tag{3}$$

If θ is considered constant, Eq. 3 is an ODE and can be integrated by separation of variables:

$$l = f(t) = \left[\left(\frac{R\sigma\cos\theta}{2\eta}\right) + \left(\frac{R^2}{4\eta}\right)(p_0 - p_{\text{atm}}) \right]^{\frac{1}{2}} (t)^{\frac{1}{2}} \tag{4}$$

and can be rearranged as:

$$\cos\theta = \left(\frac{4\eta}{R\sigma}\right) \left[lu - \left(\frac{R^2}{4\eta}\right)(p_0 - p_{\text{atm}}) \right] \tag{5}$$

where u is the instantaneous velocity of the air–liquid interface. Assuming hydrostatic pressure within the reservoir is negligible, Eq. 5 can be simplified to a form of the Washburn equation (Washburn 1921; Hilpert 2009) as follows:

$$l^2 = \frac{\sigma R t}{2\eta} \cos\theta \tag{6}$$

where l is the liquid penetration length.

For small time scales, however, the velocity predicted by Washburn equation approaches infinity as $t \rightarrow 0$. An alternative model was presented by Adams and White (2008) for surface-tension-driven flow in capillaries of arbitrary cross section. The liquid penetration length in the model by Adams and White for flows with wall friction is defined as:

$$l = \left\{ 2t_{\text{chr}} \left(\frac{p_0}{\rho} + \frac{2\sigma\cos\theta}{\rho R} \right) (t - t_{\text{chr}}[1 - \exp(-t/t_{\text{chr}})]) \right\}^{\frac{1}{2}} \tag{7}$$

where ρ is the fluid density and t_{chr} is the characteristic time of the system provided by:

$$t_{\text{chr}} = \frac{\rho R}{C\mu} \tag{8}$$

where C is a constant depending on the geometry of the cross section of the microchannel (Adams and White 2008). Neglecting hydrodynamic effects, Eq. 7 can be differentiated with respect to time resulting in the following expression (Adams and White 2008):

$$u = u_{\text{chr}} \left(\frac{\sqrt{2t_{\text{chr}}}}{2} \right) \left[\frac{1 - \exp(-t/t_{\text{chr}})}{[t - t_{\text{chr}}(1 - \exp(-t/t_{\text{chr}}))]^{1/2}} \right] \tag{9}$$

where u_{chr} is a characteristic velocity defined as:

$$u_{\text{chr}} = \left(\frac{2\sigma\cos\theta}{\rho R} \right)^{1/2} \tag{10}$$

For larger time scales and constant contact angles, Eq. 7 reduces to the Washburn equation (Adams and White 2008).

3 Experimental

3.1 Microfluidic chips

PDMS (Sylgard, Dow Corning Corporation, Midland, MI) chips were fabricated using the established soft lithography technique (Duffy et al. 1998; Whitesides and Stroock 2001). Five different chip designs were used in the experiments. The first chip design consisted of a 10-mm long straight channel. Two openings for fluidic and electrode access were punched at the ends of the microchannel. The second design consisted of a group of five straight channels with lengths of 10, 14, 18, 22, and 25 mm, separated 7 mm from each other. Each channel in this chip included two punched holes for electrodes and fluids access. The third design consisted of a serpentine microchannel with eight 90° elbows and a total channel length of 20 mm. The cross-sectional area of all the microchannels was 250 μm by 250 μm. A fourth design consisted on a star-shape microfluidic chip, having three 3.5-mm long microchannels converging into a single 7-mm long microchannel. The distal end of every microchannel was connected to a reservoir. The cross-sectional areas of all the microchannels in this design were 50 μm by 50 μm. The fifth chip design consisted of a Y-shape chip with two converging microchannels ending in a common single channel. The converging microchannels and the common outlet channel in this chip were 3.5 and 6.5 mm in length, respectively, and the microchannels were 50 μm by 50 μm. Thin PDMS layers were separately cast over a clean silicon wafer (Silicon Quest International, Santa Clara, CA). With the exception of the integrated microelectrode chip, all chips were irreversible bonded to a piece of the thin PDMS layer by oxygen plasma exposure. After bonding the chips were baked for at least 6 h at 85°C to ensure a uniform hydrophobic initial surface condition.

3.2 Dye solutions

Dye solutions for visualization experiments were prepared by diluting concentrated commercial brilliant blue (E133),

yellow (E102) and allura red (E129) food dyes (McCormick, Baltimore, MD) and ultrapure water (Millipore, Billerica, MA). The dye solutions were filtered with 0.45 μm PVDF membrane syringe-driven filters (Millipore, Billerica, MA) prior the experiments. The conductivity and pH of the resulting diluted dye solutions were measured using an Oakton Con 6 conductivity meter (Oakton Instruments, Vernon Hills, IL) and a pH5 Acorn series pH meter (Oakton Instruments, Vernon Hills, IL). The conductivities of the blue, yellow, and red solutions were 530, 480, and 510 $\mu\text{S}/\text{cm}$, respectively. The pH of all solutions was 7.5.

3.3 Integrated microelectrode

In order to demonstrate applicability of the method in integrated lab-on-a-chip applications, liquid actuation was achieved using an integrated microelectrode. Gold microelectrodes were fabricated using conventional gold wet etching technique as follows. A commercial glass slide with a 100-nm gold layer and a 5-nm chromium adhesion layer (EMF Corp., Ithaca, NY) was spin-coated with SU8-25 photoresist (MicroChem, Newton, MA). Next, the slide was prebaked at 65°C for 3 min and then baked at 95°C for 10 min. After cooling, a mask with the microelectrodes patterns was placed over the coated glass slide and exposed to UV light for 140 s, followed by post-bake steps at 65 and 95°C for 3 and 15 min, respectively. The photoresist pattern was developed using SU8 developer (MicroChem, Newton, MA). The slides were then placed in a gold etching solution made prior to the electrodes fabrication by mixing 8 g of KI and 2 g of I_2 in 80 ml of water. An 8% to 22% (v:v) solution of acetic acid to ceric ammonium nitrate was then used to remove the chromium adhesion layer. The remaining photoresist on top of the gold pattern was removed using NanoTM Remover PG (MicroChem, Newton, MA) and IPA. A single conductor copper stranded 24-gauge wire (Pico Wire, Canada) was then connected to the microelectrode using conductive epoxy (MG Chemicals, Vancouver, BC, Canada).

3.4 Experimental setup

Figure 1a shows a schematic representation of the experimental setup. The experimental configuration, with a liquid inside the microchannel, a ground electrode underneath the inlet and the corona electrode in the outlet, is shown in Fig. 1b. Figure 1c shows a picture of the experimental setup used in this study. As shown in the picture, an electrically isolated working surface was used for the experiments. The surface was a 1/4-inch thick PMMA plate with a 2-mm diameter circular opening fixed to an optical table using four rods. The circular opening in the surface

was used for ground electrode access. A corona handheld device (Electro-Technic Products Inc., Chicago, IL) which produces a voltage of 10–50 kV at 4–5 MHz was fixed to the optical table using a stand-rod holder. A Logitech Pro900 digital webcam (Logitech, Fremont, CA) and a Miro4 high-speed CCD camera (Vision Research, NJ) were used for video acquisition. A Nikon D60 digital SLR (Nikon, Tokyo, Japan) was used for still image acquisition. Figure 1c shows the experimental setup with the webcam. It is important to note that although the electrical current is limited, the electromagnetic field in the vicinity of the high frequency and high voltage electrode can disturb electronics and digital cameras in particular. For this reason, imaging at a distance was required. Specifically, 10 cm between the camera chip and the electrode was found to be sufficient while providing sufficient image data.

4 Results and discussion

4.1 Ground-directed electric discharge liquid actuation

Microfluidic liquid actuation through ground-directed electric discharge is enabled by a change in surface energy at the solid–liquid interface. The instantaneous surface oxidation caused by the plasma generated by the electric discharge results in a reduction of the liquid–gas interface contact angle at the solid. In a common sessile droplet system, the surface energy change caused by the electric discharge is manifested by a sudden and dramatic spreading of the droplet over the substrate. Figure 2 shows an ultrapure water droplet on a planar PDMS surface exhibiting a contact angle of 122° prior to exposure to the electric discharge. Following exposure the surface becomes highly wetting, exhibiting a contact angle approaching zero (<5°). The contact angles for each case were measured

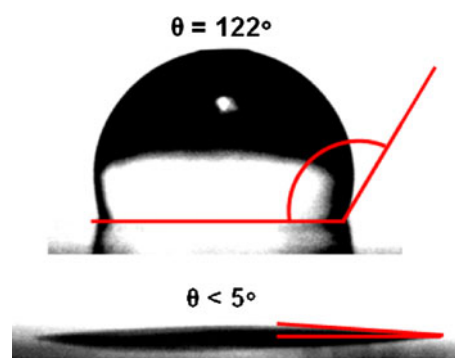


Fig. 2 Images of a nanopure water droplet on a flat PDMS surface prior and after the application of an electric discharge. The contact angles of the droplet-on-PDMS system were measured using low bond axisymmetric drop shape analysis, resulting in values of 122° for the initial condition and <5° after the surface treatment

using low bond axisymmetric drop shape analysis through Image J software.

Figure 3a presents the schematics of the first experimental configuration. A simple straight microchannel was employed. The inlet reservoir was filled with blue dye solution and the ground electrode was positioned underneath the inlet reservoir, within 1 mm of the bottom PDMS surface of the chip. The wire electrode from the corona device was placed in the outlet. The corona device was then started causing the ionization of the air surrounding the wire electrode. As shown schematically in Fig. 3a, an electric discharge and a distinctive glow from the air ionization is guided along the channel to the liquid interface, and exits the chip below the inlet reservoir to reach the ground electrode.

Figure 3b shows an image sequence of the experimental results. As shown, the directed electric discharge and subsequent surface energy change resulted in the rapid advance of the liquid along the microchannel (movie of this experiment is available in Online Resource 1). By $t = 0.006$ s following the application of the electric discharge, the liquid had advanced into the microchannel. As shown in the magnified portions inset in Fig. 3b, the initial wetting pattern mirrored the visualized electric discharge. The channel was half-filled by $t = 0.04$ s, and completely filled by 0.2 s representing an average velocity of ~ 7 cm/s.

Figure 4 shows the liquid velocity data determined from the imaging experiments and comparison with that predicted from the theoretical models. The liquid meniscus position was recorded with the high-speed CCD camera at 600 frames per second and a resolution of 800 by 600 pixels. Instantaneous velocities at different lengths along the microchannel were then calculated using a post-processing imaging software (Vision Research, NJ). These experimental results were compared with the two theoretical models described in Sect. 2, using Eqs. 6 and 9. The value of contact angle in each theoretical model was used as a fitting parameter to compare with the experimental data. Both the scaling exponent and the constant from the power law curve trend from the theoretical models were used to obtain the best fit to the experimental data for a given contact angle. The Washburn model, Eq. 6, and the model presented by Adams, Eq. 9, show a best fit at a contact angle of 65° . As expected from theory, the velocity of the liquid front reduces as it penetrates the microchannel and shows a power law dependence on time. The theoretical models and experimental data agreed within 5% for each case. This agreement suggests the PDMS surfaces had uniform wetting conditions prior to testing. It is important to note that the post-treatment surface conditions in the channel are different than those for the sessile droplet discussed above. Differences in the treatment are primarily due to the variations in field intensity and geometry in the

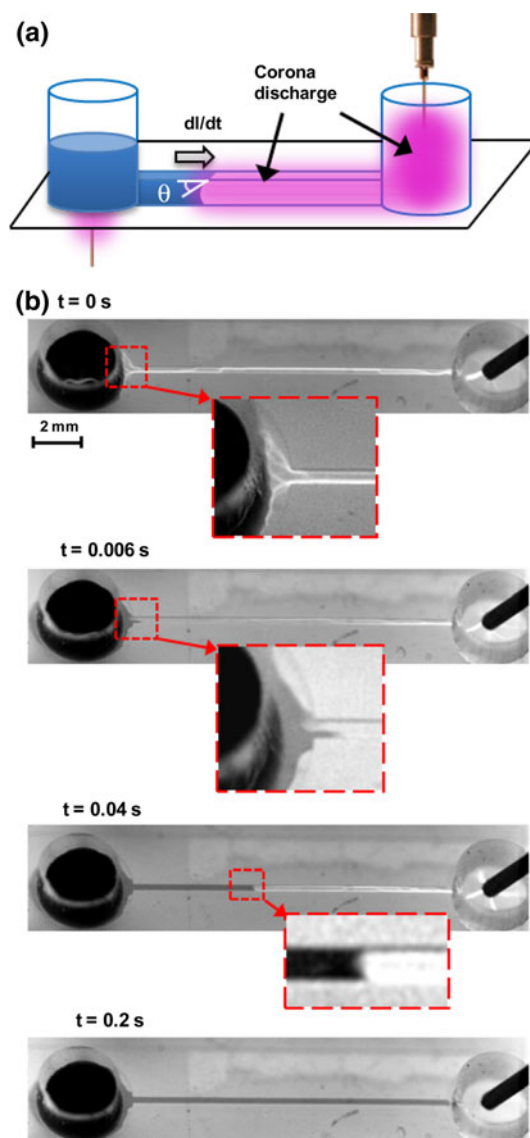


Fig. 3 **a** Schematic showing the path of a ground-directed electric discharge. After the electric discharge application, the PDMS surface becomes wetting, enabling the transport of the liquid through the microchannel by capillary action. **b** Images of an experiment demonstrating microfluidic actuation through ground-directed electric discharge. The selected pictures are part of a sequence acquired at 600 frames per second using the high-speed camera. The electric discharge is observed as it travels along the microchannel walls, ionizing the air inside, treating the surface, and subsequently enabling liquid transport. Details at the liquid–gas interface are shown *inset*. A movie of the experiment is available in Online Resource 1

two cases. It was not possible to get highly accurate direct measurements of the contact angle in the channels due to imaging artifacts. However, the observed contact angles are in line with those determined from the resulting transport. Also, the most important measure of surface treatment, in the context of this work, is the extent to which transport is enabled in the microchannel.

The dependence of the surface treatment on the length and the power of the corona discharge device are investigated in the following sections.

4.2 Influence of channel length

The dependence of the length of channel over which the electric discharge is applied was investigated using the chip with five parallel straight microchannels, as shown in Fig. 5. The inlets of each of the micro-channels were filled with dyed solution. The ground electrode was placed at the inlet and the wire electrode from the corona device at the outlet. An electric discharge, lasting approximately 0.2 s, was applied to each of the channels at a time. Liquid actuation was achieved only in the three shorter micro-channels, as shown in Fig. 5. Under these conditions, the maximum length for achieving liquid actuation was found to be 18 mm. Importantly, longer lengths may be achieved at higher power intensities or longer applications of the electric discharge. However, these results show that sub-second applications of discharges, at the relatively low power intensities used here can actuate fluids over length-scales on the order of ~ 1 cm. The influence of power intensity is considered below.

4.3 Influence of power intensity

The influence of the electric discharge power intensity on the fluid velocity was investigated. Figure 6 shows the total average velocities as a function of power intensity. The length of the microchannels used in this experiment was 18 mm and the cross section was $250 \mu\text{m} \times 250 \mu\text{m}$. Due to the lack of a quantitative power indicator in the portable

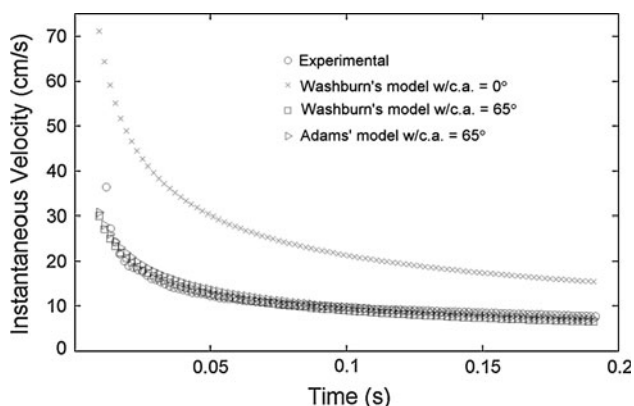


Fig. 4 Instantaneous velocities achieved through electric-discharge-induced flow. Theoretical models are used to fit the experimental data collected through imaging (in Fig. 3). Both models exhibit a best fit at a contact angle is 65° . The microchannel used in the experiment was 14 mm in length

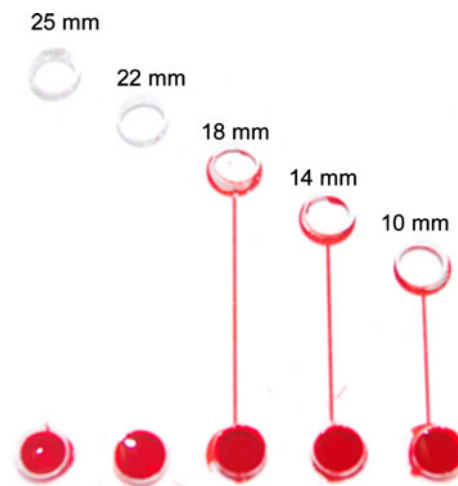


Fig. 5 Influence of channel length in ground-directed electric discharge liquid actuation. A fixed power intensity level was applied in five microchannels with lengths indicated. Liquid actuation was achieved in the three shorter microchannels, suggesting the spatial treatment is limited at a given power intensity and duration

corona device used in this study, a relative power intensity level scheme was required. The power levels were set by turning increments of 45° on the knob from a set base position. The total average velocity of the liquid transported through the channel was calculated using visualization techniques with the experimental setup shown in Fig. 1c. Figure 6a shows the average velocities at different relative power levels. The average liquid flow velocity increased linearly with the power intensity, however, relatively little change ($\sim 20\%$) was observed over the full scale of powers tested. Figure 6b shows the average effective contact angle, calculated from Washburn's equation using the observed velocities, as a function of power intensity. As shown, the contact angle resulting from the treatment decreases linearly with power intensity. As the power increases, the average effective contact angle decreases at a rate of $\sim 0.73^\circ$ per relative intensity level. Although the simple knob adjustment on the device is not quantitative, these results indicate that once ground-directed discharge is achieved, differences in surface condition achieved with further increasing power through this control are negligible. That is, a sufficient power setting was required to initiate the discharge, and further increases in the power setting of the device showed little change in the resulting treatment and flow actuation.

4.4 Application in non-straight microchannels

Microfluidic chip applications rarely involve exclusively straight microchannels. Figure 7 shows the application of ground-directed electric discharge liquid actuation to a serpentine channel structure. The experimental setup and

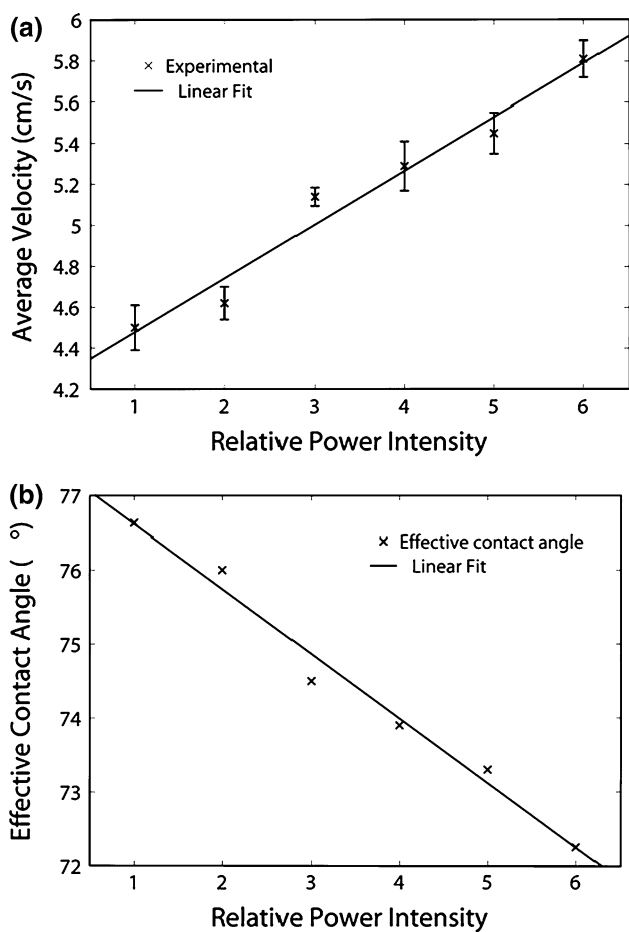


Fig. 6 **a** Average liquid velocities as a function of relative power intensity. The intensity was increased by advancing the knob of the handheld corona device 45° at each level. **b** Corresponding effective contact angle obtained by fitting the experimental data to the Washburn theoretical model

experimental procedures were otherwise similar to those employed previously. As visualized in the images in Fig. 7, the electric discharge followed the channel through eight 90° turns in a relatively long (2 cm) channel, and provided sufficient surface treatment to initiate flow back to the outlet. A movie of this experiment is available in Online Resource 2. The time required from the initiation of the discharge to the completed filling of the channel was approximately 1.3 s. The results clearly indicate that this method is readily applicable to non-straight microchannel geometries.

4.5 Application in liquid routing

Figure 8a shows a schematic representation of the star-shaped chip design used to demonstrate directed sequential liquid routing, through ground-directed electric discharge. In this experiment, the ground electrode was placed at the

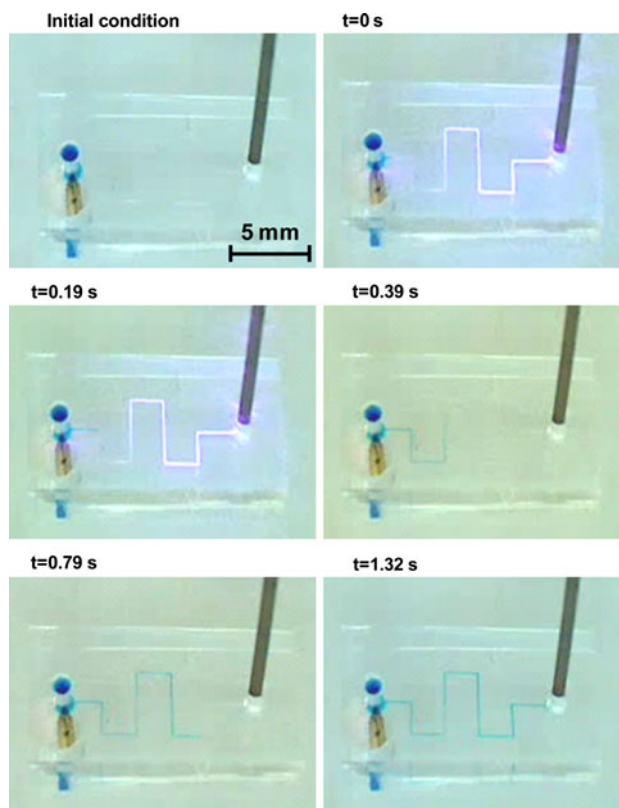


Fig. 7 Ground-directed electric discharge liquid actuation in a non-straight microchannel. The channel has eight 90° elbows and a total length of 20 mm. The discharge provided sufficient surface treatment to initiate flow back to the outlet in ~1.3 s. A movie of the experiment, at 0.25× speed, is available in Online Resource 2

divergence point, underneath the bottom PDMS layer of the hydrophobic microfluidic chip. The corona electrode was placed successively at each reservoir of the chip to route the liquid through each corresponding channel. Figure 8b shows the image sequence of the liquid routing experiment. The first electric discharge, applied at the inlet, resulted in liquid actuation along the microchannel with a penetration length equal to the distance between electrodes. Two aspects are noteworthy here: this actuation configuration is opposite that shown in the previous figures as the discharge is applied to the liquid directly and then directed through the channel; and no liquid transport in the other three microchannels resulted from this discharge. The corona electrode was then placed at an outlet and a second discharge was applied. This application resulted in the preferential transport of the liquid along the corresponding microchannel, linking the reservoir to the inlet reservoir. The third and fourth discharges routed fluid from the intersection to the remaining outlet reservoirs. A movie of experiment is available in Online Resource 3. The individual channel actuation achieved in this experiment demonstrates the potential of the ground-directed electric

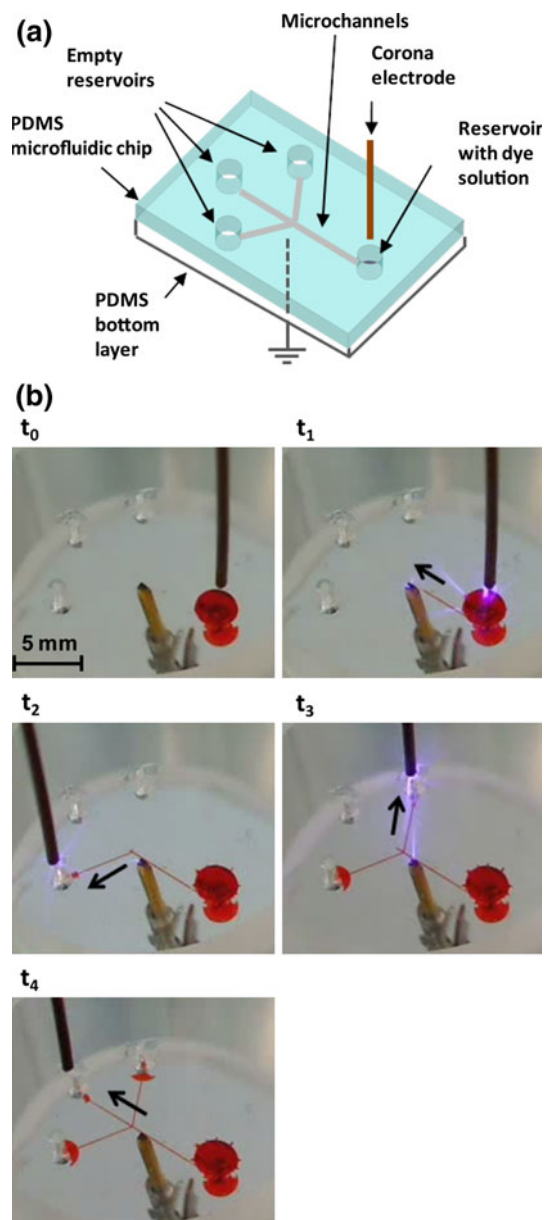


Fig. 8 Application in liquid routing. **a** Schematic representation of the star-shaped microfluidic configuration used in the experiment. The ground electrode was placed below the chip at the divergence point. **b** Image sequence of the experiment. The electric discharge was applied successively at each reservoir of the chip to route the liquid through each corresponding channel. A first discharge, applied at the inlet, resulted in liquid actuation along the microchannel with a penetration length equal to the distance between electrodes (this application of discharge at the liquid reservoir is opposite that of Fig. 1). A second discharge applied at an outlet reservoir resulted in the preferential transport of the liquid along the corresponding microchannel, linking that reservoir to the inlet reservoir. The third and fourth discharges routed fluid from the intersection to the remaining outlet reservoirs. A movie of experiment is available in Online Resource 3

discharge actuation technique for controlled preferential routing of liquid samples in complex microfluidic systems and lab-on-a-chip devices.

4.6 Ground-directed electric discharge liquid actuation to initiate solution mixing

Figure 9 shows the Y-shape chip and experimental configuration used in a mixing process initiated through ground-directed electric discharge liquid actuation. Figure 9a shows the initial configuration, having one inlet filled with yellow dye solution and the second inlet with blue dye solution. The ground electrode was placed underneath the bottom PDMS layer of the chip, at the channels' intersection, while the corona electrode was placed at the outlet. Figure 9b shows the results of the mixing process initiated by the electric discharge. After a discharge was applied, both dye solutions flowed through their respective channels to the intersection, and mixed on the way to the outlet reservoir, as indicated by the green hue in the channel and outlet. It is noteworthy that in this case, the treated region reached beyond the ground-directed channel sufficiently to induce wetting in both adjacent 3-mm channels. This was achieved by applying a higher power discharge over a longer period (6, >1 s). The residence length for diffusive mixing for this flow rate was on the order of ~ 3 mm, and the mixing channel length was 6 mm. This experiment demonstrates completion of an individual unit operation relevant to lab-on-chip applications. To integrate many such operations on a chip, delivery of the actuation via integrated microelectrodes would be required, and is demonstrated next.

4.7 Ground-directed electric discharge liquid actuation with an on-chip integrated microelectrode

Figure 10 shows the gold microelectrode fabricated on a gold-on-glass substrate, using a wet etching technique (as described in the experimental section). The resulting microelectrode had a 4-mm long tip with average width of $70 \mu\text{m}$. A single-channel microfluidic chip was placed over the glass substrate, having one of the reservoirs, the outlet, positioned over the tip of the microelectrode. The inlet was filled with blue dye solution and the ground electrode placed underneath the glass substrate. A discharge was remotely applied to the microelectrode via a 24-gauge wire resulting in the liquid transport of the dye solution through the microchannel, as shown in Fig. 10 (movie of experiment is available in Online Resource 4). The liquid reached the outlet after 0.4 s, resulting in an average fluid flow velocity of 4.7 cm/s, in agreement with results achieved using the handheld corona device directly. This experiment demonstrates the flexibility of the ground-directed electric discharge liquid actuation technique and its potential for on-chip integration. Additionally, wetting-based techniques are applicable to a range of fluids of interest in microfluidic systems. Most

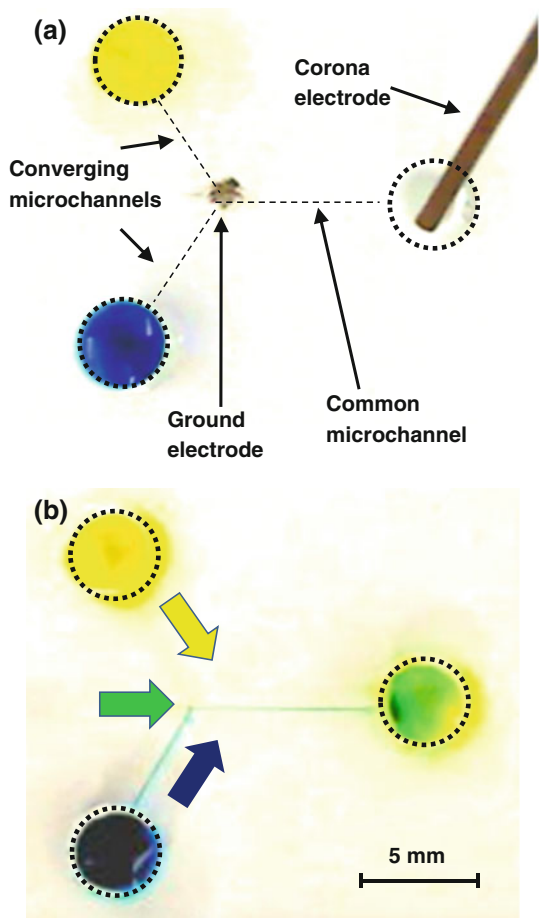


Fig. 9 Ground-directed electric discharge liquid actuation to initiate solution mixing. **a** The two inlets in the Y-shape chip were filled with light (shown yellow online) and dark (shown blue online) dye solutions. The ground electrode was placed underneath the intersection from the converging channels, and the corona device electrode was placed at the outlet. **b** Image of the resulting liquid mixing process initiated by electric discharge liquid actuation. After an electric discharge was applied, both dye solutions flowed through their respective channels to the intersection, and mixed on the way to the outlet reservoir, as indicated by the intermediate hue (shown green online) in the channel and outlet

notably, the ability to direct fluids using on-chip electrodes presents opportunities to achieve highly multiplexed, programmable fluidic functions through this technique. It is also important to note that, for applications in the biomedical field, we foresee minimal damage to biological samples as the field is chiefly applied to the gas in the microfluidic system, and as the field application time is very short. The relatively simple control methods developed here have potential to be integrated at high density to provide for much more complicated functions. Analogously, relatively simple pneumatically actuated microfluidic valve structures have enabled a vast array of complex on-chip processes.

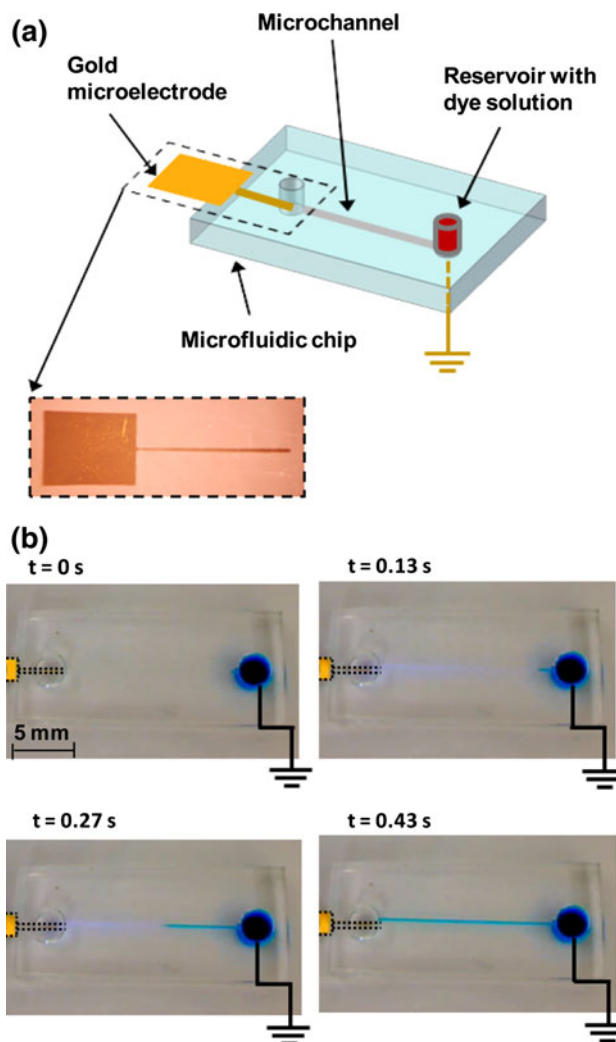


Fig. 10 Ground-directed electric discharge liquid actuation with an on-chip integrated microelectrode. **a** Schematic representation of the single-channel microfluidic chip with an integrated gold microelectrode used in the experiment. The tip of the microelectrode was 4 mm in length and had a width of $\sim 70 \mu\text{m}$. The outlet reservoir was filled with dye solution and a ground electrode was placed underneath, as previously. A picture of the microelectrode is shown as an inset. **b** Sequence of images showing electric discharge liquid actuation with an integrated microelectrode. The liquid reached the outlet after 0.4 s, resulting in an average fluid flow velocity of 4.7 cm/s, in agreement with results achieved using the handheld corona device directly. A movie of the experiment is available in Online Resource 4

5 Conclusions

In this study, a novel liquid actuation technique using a ground-directed electric discharge was demonstrated. High-speed visualization analysis of discharge-induced liquid flows in straight microchannels indicated velocities up to 7 cm/s. Two theoretical models were used to fit the experimental data, finding a best fit at a contact angle of 65° . Fluid flow velocities exhibited a linear dependence on microchannel length. The increase in power setting of the

device showed a minimal change in the resulting treatment and flow actuation. We found that longer lengths may be achieved at higher intensities or longer exposure times. Together these results show that sub-second applications can actuate fluids over length-scales on the order of ~ 1 cm. The average liquid flow velocities were found to increase linearly with the power intensity, with average flow velocities in the order of ~ 5 cm/s. The potential of this technique for integrated lab-on-a-chip applications was also demonstrated by application in a serpentine channel structure, for on-demand fluid routing, to initiate a mixing process, and through an on-chip integrated microelectrode. Still, when these demonstrations involve basic fluidic actuation and routing, the combination, integration, and multiplexing of these operations may be used to achieve applications with higher level of complexity. The applications shown here demonstrate the ability to complete and control individual unit operations relevant to lab-on-chip applications in diverse microchannel geometries, and to effectively direct fluids to achieve highly multiplexed, programmable fluidic functions.

Acknowledgments The authors would like to acknowledge funding from the Canada Research Chairs Program as well as a scholarship to CE and a research grant to DS from the Natural Science and Engineering Council of Canada (NSERC). Infrastructure funding from the Canadian Foundation for Innovation is also gratefully acknowledged. The authors would also acknowledge helpful discussions with Te-Chun Wu.

References

- Adams TM, White AR (2008) Macroscopic conservation equation based model for surface tension driven flow. *Adv Fluid Mech* 7(1):133–141
- Arifin DR, Yeo LY, Friend JR (2007) Microfluidic blood plasma separation via bulk electrohydrodynamic flows. *Biomicrofluidics* 1(1):014103–014113
- Bittencourt JA (2004) *Fundamentals of plasma physics*. Springer, New York
- Chih-Peng H, Jewell-Larsen NE, Krichtafovitch IA, Montgomery SW, Dibene JT, Mamishev AV (2007) Miniaturization of electrostatic fluid accelerators. *J Microelectromech Syst* 16(4):809–815
- Duffy DC, McDonald JC, Schueller OJA, Whitesides GM (1998) Rapid prototyping of microfluidic systems in poly(dimethylsiloxane). *Anal Chem* 70(23):4974–4984
- Evju JK, Howell PB, Locascio LE, Tarlov MJ, Hickman JJ (2004) Atmospheric pressure microplasmas for modifying sealed microfluidic devices. *Appl Phys Lett* 84(10):1668–1670
- Fair RB (2007) Digital microfluidics: is a true lab-on-a-chip possible? *Microfluid Nanofluid* 3(3):245–281
- Haubert K, Drier T, Beebe D (2006) PDMS bonding by means of a portable, low-cost corona system. *Lab Chip* 6(12):1548–1549
- Hilpert M (2009) Effects of dynamic contact angle on liquid infiltration into horizontal capillary tubes: (Semi)-analytical solutions. *J Colloid Interface Sci* 337(1):131–137
- Hilpert J, Kern J (1974) Electric wind in a corona discharge—theory and measurement. *Arch Elektrotech* 56(1):50–54
- Horiuchi K, Dutta P (2006) Electrokinetic flow control in microfluidic chips using a field-effect transistor. *Lab Chip* 6(6):714–723
- Hsu CP, Jewell-Larsen NE, Krichtafovitch IA, Montgomery SW, Dibene JT, Mamishev AV (2007) Miniaturization of electrostatic fluid accelerators. *J Microelectromech Syst* 16(4):809–815
- Juncker D, Schmid H, Drechsler U, Wolf H, Wolf M, Michel B, de Rooij N, Delamarque E (2002) Autonomous microfluidic capillary system. *Anal Chem* 74(24):6139–6144
- Kim J, Chaudhury MK, Owen MJ (2000) Hydrophobic recovery of polydimethylsiloxane elastomer exposed to partial electrical discharge. *J Colloid Interface Sci* 226(2):231–236
- Kim J, Kido H, Rangel RH, Madou MJ (2008) Passive flow switching valves on a centrifugal microfluidic platform. *Sens Actuators B* 128(2):613–621
- Luk VN, Wheeler AR (2009) A digital microfluidic approach to proteomic sample processing. *Anal Chem* 81(11):4524–4530
- Makamba H, Kim J, Lim K, Park K, Hahn JH (2003) Surface modification of poly(dimethylsiloxane) microchannels. *Electrophoresis* 24(21):3607–3619
- Moreau E (2007) Airflow control by non-thermal plasma actuators. *J Phys D* 40(3):605–636
- Robinson M (1962) A history of electric wind. *Am J Phys* 30(5):366
- Seimandi P, Dufour G, Rogier F (2009) An asymptotic model for steady wire-to-wire corona discharges. *Math Comput Model* 50(3–4):574–583
- Sun C, Zhang D, Wadsworth LC (1999) Corona treatment of polyolefin films—a review. *Adv Polym Technol* 18(2):171–180
- Sung Kwon C, Hyejin M, Chang-Jin K (2003) Creating, transporting, cutting, and merging liquid droplets by electrowetting-based actuation for digital microfluidic circuits. *J Microelectromech Syst* 12(1):70–80
- Thorsen T, Maerkl SJ, Quake SR (2002) Microfluidic large-scale integration. *Science* 298:580–584
- Thorslund S, Nikolajeff F (2007) Instant oxidation of closed microchannels. *J Micromech Microeng* 17(4):N16–N21
- Unger MA, Chou HP, Thorsen T, Scherer A, Quake SR (2000) Monolithic microfabricated valves and pumps by multilayer soft lithography. *Science* 288:113–116
- Washburn EW (1921) The dynamics of capillary flow. *Phys Rev* 17(3):273
- Whitesides GM (2006) The origins and the future of microfluidics. *Nature* 442(7101):368–373
- Whitesides GM, Stroock AD (2001) Flexible methods for microfluidics. *Phys Today* 54(6):42–48
- Yeo LY, Hou D, Maheshwari S, Chang HC (2006) Electrohydrodynamic surface microvortices for mixing and particle trapping. *Appl Phys Lett* 88(23):233512
- Zenkiewicz M (2005) Oxidation of the filled-polyolefin-film surface layer by corona treatment. *Przem Chem* 84(10):733–739